Observational Study of the Atmospheric Boundary Layer over Antarctica

ZBIGNIEW SORBJAN*, YUJI KODAMA AND GERD WENDLER

Geophysical Institute, University of Alaska, Fairbanks, AK 99775

(Manuscript received 1 June 1985, in final form 19 October 1985)

ABSTRACT

During the austral summer of 1982/83, measurements of wind and temperature profiles were made through the atmospheric boundary layer in Adelie Land, East Antarctica, an area known for strong katabatic winds. It was found that a shallow but strong temperature inversion was developed at night, and destroyed during the day, resulting in the development of a well-mixed layer. Wind hodographs were quite regular and spiral-like at night, but irregular during the day. The mean wind direction was about 40° to the left, looking downslope, but more downslope at night and more cross-slope during the day.

The conclusion was derived that during the polar summer the flow over Antarctica is controlled by the gravitational factor (slope-induced baroclinicity), by the thermal stability (turbulent mixing), and also by the synoptic forcing.

1. Introduction

No other single phenomenon has such a strong influence on the climate of a whole continent as the katabatic winds have on Antarctica. Although flows over slopes of Antarctica have been investigated for many years (e.g., Ball, 1957; Mather and Miller, 1967a,b; Schwerdtfeger, 1970; Radok, 1973), the past studies have been restricted by the lack of observational data, especially on the vertical structure of katabatic winds.

The overall picture of katabatic flow, existing in the literature, was mainly obtained from observations performed at a few inland stations in Antarctica. A number of studies employed series of wind soundings at Byrd, South Pole and Vostok (e.g., Lettau and Schwerdtfeger, 1967; Artemyev, 1972). Some investigations used data from Plateau Station with a well-instrumented, 32-m tower (Lettau et al., 1977; Kuhn et al., 1977; Riordan, 1977). In Adelie Land, Delaunay and Poggi (1981) conducted measurements, using a 70-m tower at Dumont d'Urville (an island a few kilometers offshore of the continent), along with 20-m towers on the ice slopes of Adelie Land.

Out of this latter study, with the goal of obtaining a better understanding of the katabatic wind, a joint experiment was initiated between the Geophysical Institute (University of Alaska), the University of Grenoble, and later by Centre de Researches en Physique de l'Atmosphere (Poggi et al., 1982; Wendler et al., 1983). As a part of the program, in austral summer, January 1983, measurements of the wind and temperature profiles were carried out at different sites along the slope of Antarctica. The observations were supported by simultaneous measurements from five automatic weather stations (AWS), built by Stanford University and serviced by the University of Wisconsin. They were deployed previously in Adelie Land.

Our boundary layer measurements were carried out at three inland sites, where AWS sites D47, D57, and D80 are located. At the same time, the French (Sennequier et al., 1984) were performing measurements at D10, about 5 km from the ocean (Fig. 1).

The present paper discusses only the boundary layer data collected at the inland sites during the experiment. The French observations (at D10 and Dumont d'Urville) performed in the vicinity of the ocean, where the flow is strongly influenced by local features (Gosink, 1982), are not considered in our study.

2. Area and instrumentation

The geographic and climatic characteristics of the sites can be seen from Table 1. All sites were, of course, steadily covered by snow, and the topography was very uniform. In the area of D57 and D47, where the steepness of the slope increases somewhat relative to D80, well-developed sastrugi fields were found (Wendler and Kodama, 1984).

The measurements were done with an Air-Sonde system, which was developed by Atmospheric Instrumentation Research, Inc. in Boulder, Colorado. Either a kite or a balloon was used as a carrier for the Air-Sonde. The balloons were used when the wind speed was in excess of 12 m s^{-1}, because for higher wind speeds a kite could be lost. The data were telemetered

* On leave from the Institute of Environmental Engineering, Warsaw Polytechnic University, 00651 Warsaw, Poland. Present address: Dept. of Geological Geophysical Science, University of Wisconsin–Milwaukee, Milwaukee, WI.

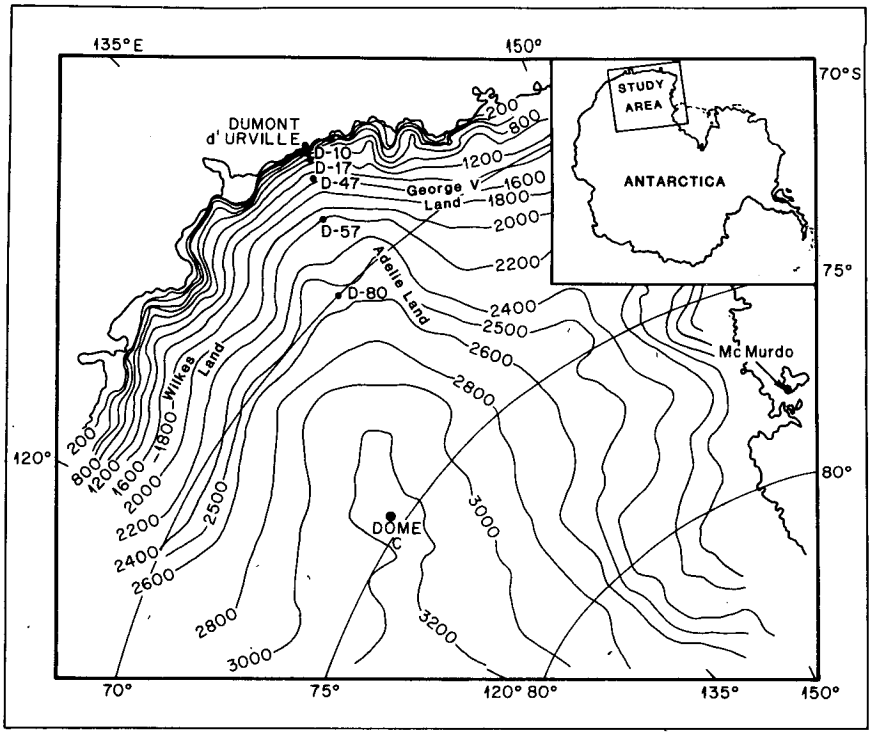

FIG. 1. Map of Antarctica.

to the ground station, and recorded on a magnetic tape. About every fourth dataset was printed out by our HP 97 calculator, so that a quality check could be made of the data while in the field. For 24-hour periods in January 1983, datasets were taken most of the time in about 6-hour intervals for each of the three stations (D47, D57, D80). Vertical soundings at these sites were not simultaneous.

The most southerly station, D80, had continuous daylight, while there was about 20 hours of daylight at D47, the most northerly station (Table 1). It should be noted that there was a prevalent, marked diurnal variation in temperature, even at D80, due to the sun elevation changes during the course of the day.

TABLE 1. The geographic and climatic characteristics at D47, D57, and D80.

Station	D80	D57	D47
Location	70°01'S 134°43'E	68°11'S 137°32'E	67°23'S 138°41'E
Height (m)	2450	2103	1560
Distance from the coast (km)	440	210	110
Slope	0.0018	0.0055	0.0065
Slope azimuth (deg. from north)	210	210	210
Period	12–14 Jan	20 Jan	23–25 Jan
Sunrise	24-h sun	0115	0230
Sunset	24-h sun	0045	2330
Mean summer temperature (°C)	−32	−20	−17
Mean summer wind (m s^{-1})	5.5	9.6	11.3

The summer (November–January) mean temperatures at the height of 3 m from the snow surface decrease when going up the slope: −17°C for D47, −20°C for D57, and −32°C for D80.

Opposite to this, the mean wind speed at the same level as those of temperatures increases when going down the slope. We found that the mean wind speeds at this level in summer are: 11.3 m s^{-1} at D47, 9.6 m s^{-1} at D57, and 5.5 m s^{-1} at D80.

The wind directional constancy, which is defined as the ratio of the magnitude of the mean wind vector to the mean wind velocity (when wind blows only from one direction, the wind constancy is equal to one; when magnitude and frequency of winds from all directions are the same, the wind constancy is zero), is quite high for all stations, with monthly values of about 0.9.

The increasing wind speed, when traveling down the slope of the Antarctic continent, keeps the equivalent chill factor (Dalrymple and Stroschein, 1966) fairly constant for the three stations, and the values in January were found to be 1500–1700. This corresponds to the chill temperature of about −50°C. These unpleasant environmental conditions, together with the drifting and blowing snow, which was experienced during about half of the time of the expedition, made measurements difficult to perform.

A summary of the collected data is given in Tables

TABLE 2. The summary of the boundary layer measurement at D80, D57, and D47 in January 1983.

Run	Location	Day in January	Time	Solar elevation (deg)	Carrier
1	D80	12	1750	29.7	kite
2	D80	12	2216	8.5	kite
3	D80	13	1111	36.6	balloon
4	D80	13	1737	30.5	balloon
5	D80	14	0026	2.3	balloon
6	D80	14	0626	13.8	kite
7	D80	14	0707	17.1	balloon
9	D80	14	1213	39.5	balloon
10	D80	14	1806	28.0	balloon
13	D57	20	1227	41.9	balloon
14	D57	20	2340	(−1.0)	balloon
17	D47	23	1852	16.4	kite
18	D47	24	0003	(−3.2)	kite
19	D47	24	0624	16.5	kite
20	D47	24	1203	41.5	kite
21	D47	24	1744	22.7	kite
22	D47	25	1029	37.5	kite

2 and 3. Seventeen vertical profiles of the wind and temperatures were obtained (9 profiles for D80, 2 for D57, and 6 for D47). All measured profiles were smoothed using a 3-point averaging operator (sometimes used more than once) to filter obtained scatter, which could not be explained physically.

Table 4 provides the additional information on weather conditions during the experiment.

3. Analysis of the temperature profiles

Our analysis is based on the vertical profiles of the temperature and wind velocity, since the direct measurements of turbulent fluxes were not available. We will start from a discussion of the time variations of the temperature field in the atmospheric boundary layer (ABL).

The observations, performed approximately every six hours at every site, enable us to observe the diurnal cycle of the potential temperature profiles. The longest series of nine profiles was obtained at D80 (Fig. 2). The general picture emerging from Fig. 2 is that the measured potential temperature profiles do not differ from those observed in lower latitudes, where a mixed layer of uniform potential temperature with height occurs during the day and a temperature inversion is observed at night (Arya, 1982). In January at D80 the day (defined as the period with a positive net radiation balance) lasts about 15 hours (see Fig. 6). Figure 2 shows that during daytime hours, a mixed layer with a height of about 200–400 m develops. This indicates a mean entrainment velocity of about $w_e = 5.6 \times 10^{-3}$ m s^{-1}. This value is one order of magnitude smaller than the typical values observed in lower latitudes and proves that the observed mixed layer is quasi steady state. Based on laboratory measurements and aircraft data, Deardorff and Willis (1974) estimated the entrainment rate w_e of about 2% of the convective velocity scale w_*. This gives a low value of $w_* \sim 0.3$ m s^{-1} in our case.

Above the mixed layer a 50–100 m thick transition layer borders with the free atmosphere. The potential temperature structure of the free atmosphere is characterized by a gradient of about 10^{-2} K m^{-1}. The strongly stratified superadiabatic layer underneath, several tens of meters deep, is a transition between the mixed layer and several degrees warmer snow surface.

Figure 2 also shows that at night, a shallow 100–200 m inversion layer rapidly develops above the surface. Its growth does not destroy the mixed layer above, which exists for the whole night and therefore can be called "nocturnal mixed layer." Radiative cooling decreases the temperature near the ground by the order of 10 K at the height of 1.5 m—the lowest level of observations (Table 3). As a result, a negative curvature of the potential temperature profile is usually observed. Only one case of positive curvature of the potential temperature profile was observed in Run 14, which is displayed in Fig. 3. According to Andre and Mahrt (1982), this indicates a relative importance of the turbulent mixing versus radiative cooling in this case.

Analysis of the potential temperature profiles enables us to determine the height of the daytime and nighttime boundary layers. The top of the stable boundary layer h was defined by the level at which the potential temperature gradient becomes constant with height. The

TABLE 3. General characteristics of the boundary layer in Adelie Land, East Antarctica.

Run	Time	ABL Height* z_i	ABL Height* h	$\theta_0 - \theta_t$†	V_0	V_t@
1	1750	**	**	**	6.5	**
2	2216	—	**	**	2.0	**
3	1111	375	—	−1.4	2.8	8.1
4	1737	400	—	−3.2	2.8	2.2
5	0026	—	175	11.3	1.5	2.6
6	0626	—	**	—	2.0	**
7	0707	50	150	10.2	2.0	4.3
9	1213	100	—	−1.6	3.1	3.8
10	1806	175	—	−1.2	2.3	2.9
13	1227	250	—	0.05	12.3	13.5
14	2340	—	225	7.0	12.0	16.4
17	1852	—	85	0.6	4.0	7.1
18	0003	—	100	4.1	4.0	6.6
19	0624	200	—	0.3	6.5	9.0
20	1203	125	—	−0.1	6.2	6.8
21	1744	100	—	0.05	6.0	7.4
22	1029	200	—	−1.0	7.3	9.5

* z_i, h: heights of daytime and nighttime ABL.
† $\theta_0 - \theta_t$: temperature difference between top and the bottom (1.5 m) of ABL.
@ V_0, V_t: wind at $z = 1.5$ m and at the top of ABL.
**: sounding did not reach to the top of the ABL.

TABLE 4. The information about cloud conditions, radiative balances, and solar elevations for the days of the measurements in Adelie Land, East Antarctica.

Day in January	Time	Cloud amount (/10)	Cloud type	Time	Radiation: Net short ($W m^{-2}$)	Radiation: Net all ($W m^{-2}$)	Solar elevation (deg)
12	2240	—	St, Sc	0910	118.6	94.2	27.7
13	1015	10	Cs, As	1015	160.4	81.6	32.8
13				1220	195.3	94.2	39.9
13	1710	5	Cs, Ci	1720	174.4	16.0	31.9
13				1847	125.6	40.5	24.7
13	2355	1	Cs, Ci	2355	9.8	−59.3	3.4
14	0547	4	Cs, As	0547	48.1	−34.2	10.9
14	0758	5	Cs, Ac	0758	131.2	40.5	21.4
14	0901	5	Ci, St				
14	1002	4					
14	1127	10	As	1127	166.0	147.2	37.3
14	1228	8	St, Sc				
14	1305	3	Ci				
14	1725	2	As	1725	153.5	144.4	31.3
20	0800	1	Ci, St	1010	159.8	50.2	36.5
20	1537	0		1545	127.7	37.7	34.2
20	1837	0		1837	60.7	0.0	19.0
20	2215	0		2215	16.0	−40.1	2.2
21	0020	0		0020	0.0	−71.9	(−1.8)
21	0600	0		0600	86.5	27.9	14.6
23	1630	8	St, Sc, Ci	1955	54.4	−12.6	10.6
23	1955	3	Cs, Ac	2315	0.0	−59.3	(−1.9)
24	0603	10	St, Sc	0745	67.0	40.5	24.3
24	1138	10	St, Sc	1138	121.4	97.0	40.9
24	1730	9	Sc	1730	80.2	62.8	24.0

top of the mixed layer z_i was defined as the height at which the potential temperature starts to increase with height. The values of the boundary layer heights were found "by eye." The definition and determination of the mixed layer height seems reasonably clear. The definition of the stable boundary layer is not unique, but one of many that are possible (Arya, 1981; Wentzel, 1982).

In Figs. 4 and 5, potential temperature profiles from all three sites, are grouped in two stability classes. Figure 4 shows the daytime profiles obtained from observations at D80 and D47. This figure indicates three distinct regions of the daytime ABL: superadiabatic surface layer, mixed layer, and above it, the transition layer to the free atmosphere. In Fig. 5, dimensionless nocturnal profiles are presented. The scaling factor ($\theta_0 - \theta_t$) is the difference between potential temperature θ_0 at the 1.5 m level and potential temperature θ_t at the top of the stable boundary layer. It is important to notice that this difference at night has much higher absolute values than during the day (Table 3).

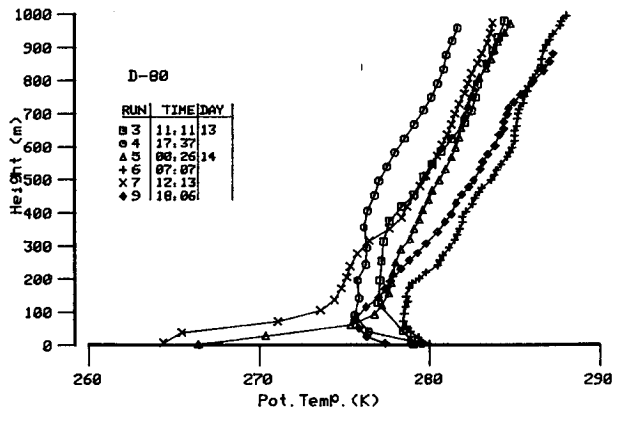

FIG. 2. Potential temperature profiles at D80.

Figure 5 indicates that dimensionless, nocturnal potential temperature profiles can be expressed in the simple exponential form $(1 - z/h)^{\alpha}$, where α is a power coefficient. This agrees with the results of Yamada (1979), who obtained the value of $\alpha = 3$. The cubic model of Yamada approximates our Run 5 profile quite well. However, Fig. 5 shows that the power α changes over a wide range of values. This is caused by nonstationarity due to the short night duration. Results from the radiative model of Cerni and Parish (1984) suggest that steady state in the inversion layer can be reached in a day or so.

A simple exponential formula does not describe the case of the transition profile (Run 7). In this case, turbulence becomes strong enough to occupy the lower part of the inversion layer. The negative curvature of the temperature profile disappears and an isothermal layer is formed above the surface.

Analysis of the Richardson number profiles (not

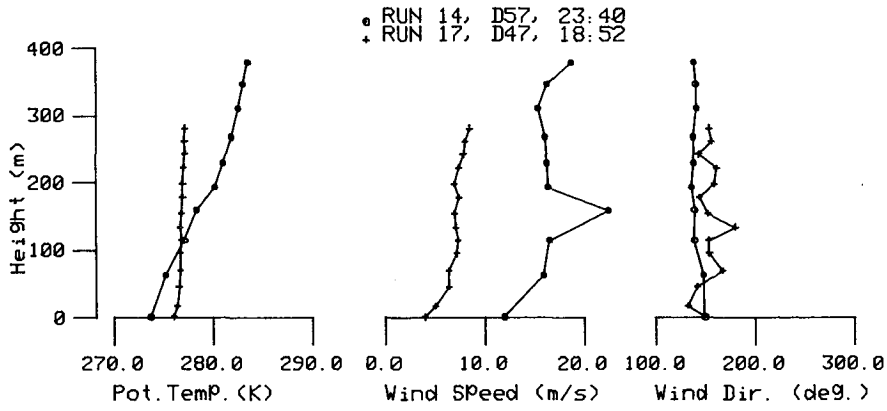

FIG. 3. Vertical profiles of the temperature and wind from Run 14 at D57 and Run 17 at D47.

shown), which have irregular sharp peaks at different heights, indicates that all nighttime cases belong to the stable-sporadic class of turbulence (Arya, 1982). The layer of continuous turbulence ($Ri < 0.25$) occurs near the surface only. The stable-continuous regime, defined as $Ri < 0.25$, in the whole boundary layer, is observed only in Run 17 (shown in Fig. 3), which is a transition between daytime and nighttime conditions. This case can also be classified as neutral, since a mixed layer occupies all the ABL, except for a shallow (25 m) surface inversion sublayer.

4. Analysis of the wind field

Surface winds in Antarctica blow from the high plateau to the edge of the continent, crossing contour lines at an angle of approximately 45° to the left of the fall line (Mather and Miller, 1967). A typical example is shown in Fig. 6 (D80, 13–14 January). The slope direction is shown in the left corner of the figure. From Fig. 6 it follows that the surface wind vector becomes more downslope at night. This effect can also be seen from Fig. 7, which displays a time variation of the mean temperature along with the mean wind speed and direction at D80 (average of the last 17 days of January). The diurnal amplitude of the wind direction in Fig. 6 is 27°, and 16° in Fig. 7. The mean wind in Fig. 6 is oriented about 40° to the left of the fall line. In Fig. 6 the diurnal changes of the potential temperature and net radiation are also shown.

Changes of the wind direction toward the maximum

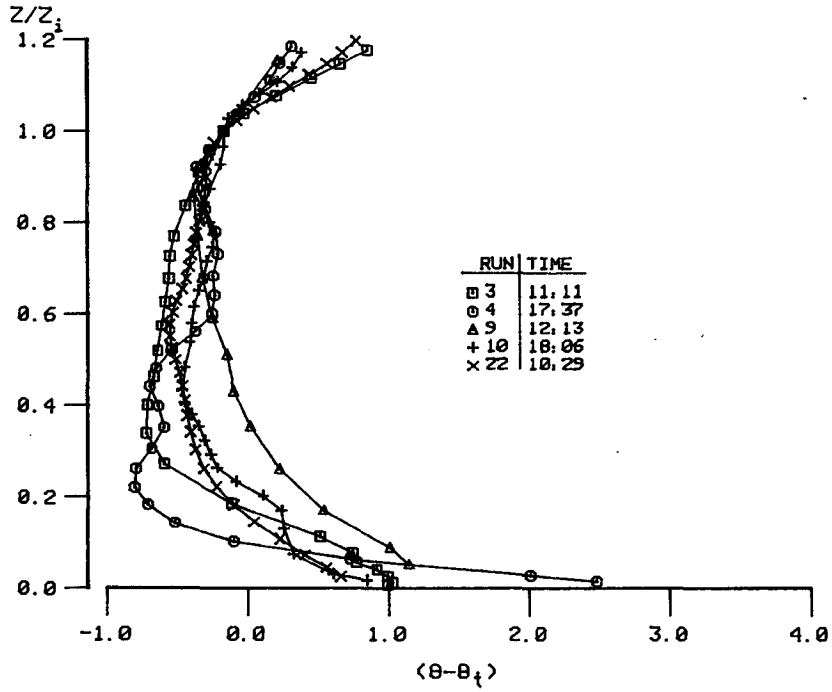

FIG. 4. Daytime potential temperature profiles.

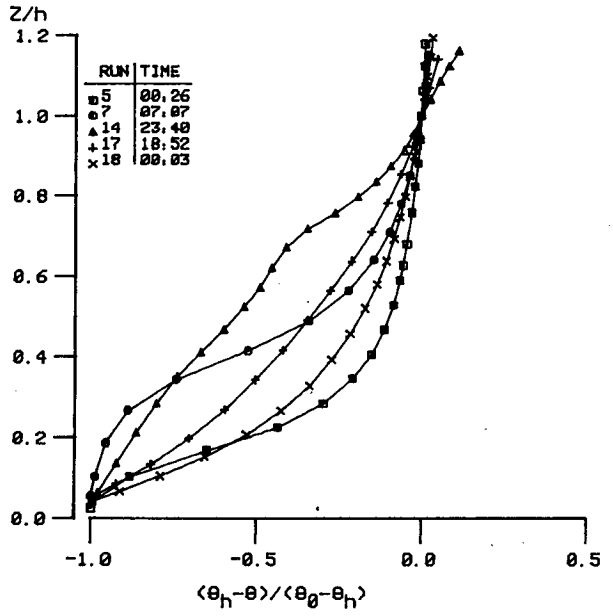

FIG. 5. Nondimensional profiles of the potential temperature at night.

slope at night, and away from it during the day are governed by the balance of three factors: gravitational, the thermal stability (turbulent mixing), and the synoptic forcing.

Gravitational forcing is caused by the thermal activity of the underlying surface over a sloping terrain. Cooling or heating of the surface generates an additional component of the geostrophic wind (thermal wind), $v_T = \beta\psi\theta'/f$, where β is the buoyancy parameter, ψ is the slope angle, θ' is the difference in potential temperature at the actual height and the top of the boundary layer, and f is the Coriolis parameter. The slope-induced thermal wind v_T is dependent on height and oriented perpendicular to the slope vector (Sorbjan, 1984). The total geostrophic wind $\mathbf{G}$ is expressed in the form:

$$\mathbf{G} = \mathbf{G}_t + [0, v_T], \tag{1}$$

where $\mathbf{G}_t$ is the synoptic geostrophic wind vector. Since v_T is positive during the day and negative at night, the total geostrophic wind vector, at the height z, turns to the left or to the right with respect to the vector $\mathbf{G}_t$.

In the case of the strong temperature inversion (and weak turbulent mixing), the negative thermal wind v_T is able to keep the surface wind vector slightly to the left, with respect to the slope vector, for all possible orientations of the flow on the top of the friction layer (Mahrt and Schwerdtfeger, 1970). This explains the persistency of the wind observed during the winter over Antarctica. However, this mechanism does not apply in the summertime.

During the summer, thermal stability and turbulent mixing play more important roles, controlling the angle between the surface and geostrophic wind. In the well-mixed layer during the day, this angle is small, since the wind vector is almost uniform, and close to the geostrophic wind vector. It is easy to find that $v_T \sim \theta'$ (for $\beta = 0.03$, $\psi = 3 \times 10^{-3}$ and $f = 10^{-4}$). Since $\theta' \sim 10$ K during the night and $\theta' \sim 1$ K during the day, it follows that the gravitational factor is important during the night, but is negligible during daytime, since it is only about 0.1 of the geostrophic wind.

The diurnal variation of the wind spirals at D80 are shown in Fig. 8. There, and on all remaining figures, the x-axis of the coordinate system is oriented down slope. The nocturnal hodographs in the figure have shapes of spirals, with wind vectors turning to the left with height. The surface wind at night is more downslope and weaker than during the day. The daytime hodographs of Runs 4 and 9 indicate that the surface wind velocity is turned more cross-slope, as an effect of stability. Close to the top of the ABL, the hodographs unexpectedly turn to the left and decrease the u-com-

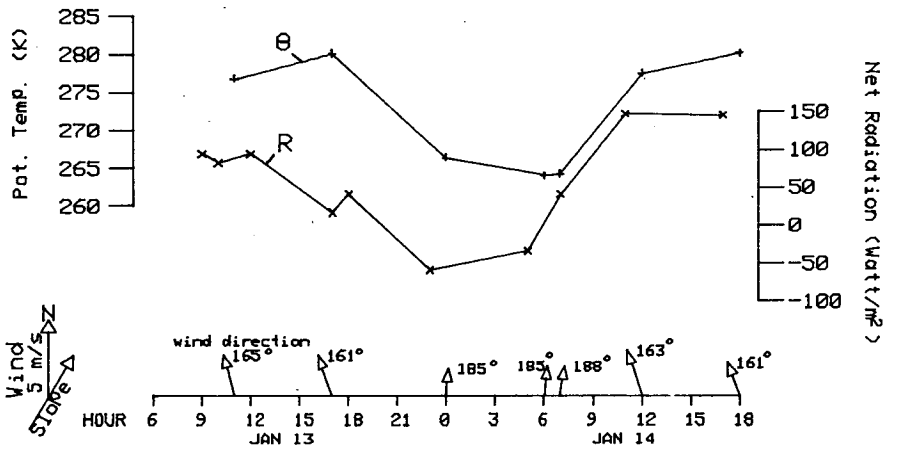

FIG. 6. Diurnal variation of the potential temperature (θ), net radiation (R), and wind velocity vector at D80.

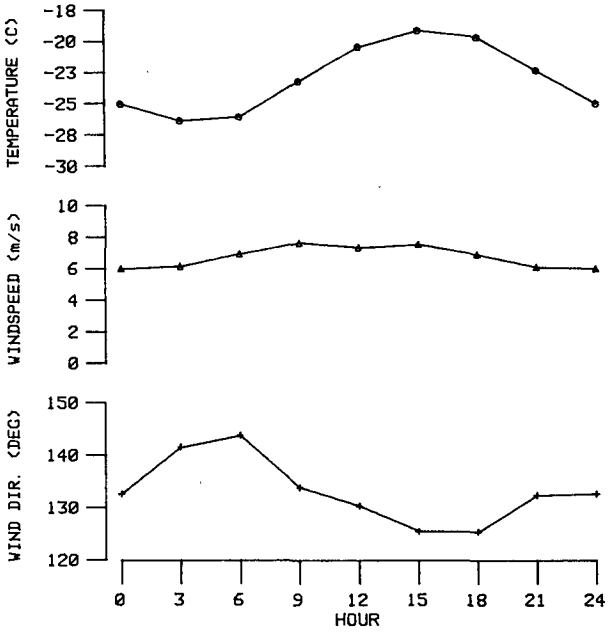

FIG. 7. Diurnal variation of the mean (17 days of January) values of the temperature and wind at D80.

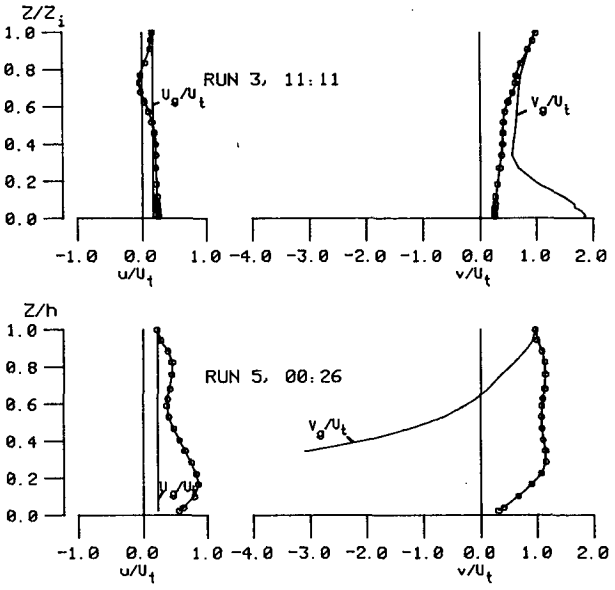

FIG. 9. Profiles of the components of the wind vector and the total geostrophic wind vector during day and night. U_t-wind velocity at the top of the ABL. U_g, V_g-components of the total geostrophic wind vector $\mathbf{G}_t$.

ponent. This can be explained as an effect of a synoptic scale baroclinicity or of secondary flows (Brown, 1981).

Characteristic features of the daytime and nighttime wind profiles are shown in Fig. 9. In this figure, the components of the total geostrophic wind, obtained from Eq. (2) are also plotted. We assumed that $\mathbf{G}_t$ is equal to the wind vector on the top of the boundary layer and is constant for the whole layer. The thermal wind is only due to the slope. The synoptic thermal wind components could not be computed. A similar procedure was previously adopted by Kuhn et al. (1977). In Fig. 9, a well-mixed, daytime profile of the wind components (Run 3) is shown to be quite uniform. The components of the nocturnal wind velocity vector increase faster with height and possess characteristic maxima.

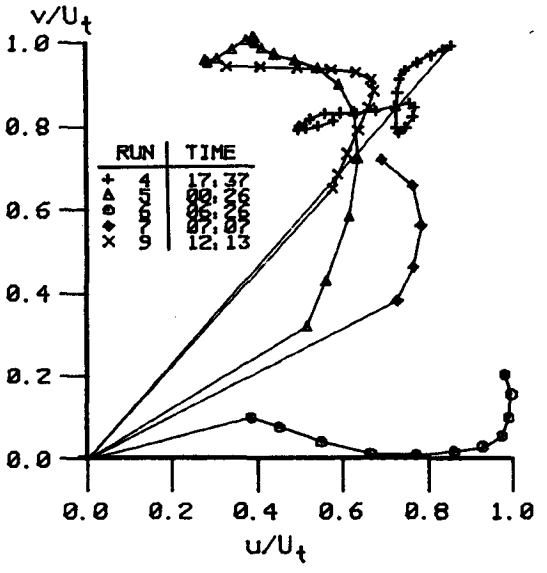

FIG. 8. Diurnal changes of wind hodographs at D80, U_t-wind velocity at the top of the ABL.

In Fig. 10, vertical wind profiles, classified into three stability regions, are presented. Profiles of the stable class (Fig. 10a) have maxima, which, however, are not pronounced and occur at different heights (z/h). The "transition" profiles (Fig. 10b) are quite regular and can be approximated by an exponential formula of the type $(z/h)^{\alpha}$. The profiles for the convective class are similar to the "transition" profiles.

5. Some theoretical and modeling considerations

In this section several conclusions will be derived by a comparison of our measurements with a simple solution of the momentum equations listed in the Appendix. These equations qualitatively express characteristic features of the ABL over Antarctica. The flow, described by these equations, is based on a balance of the Coriolis, frictional, and pressure forces (with components generated by a slope and by synoptic baroclinicity), resulting in a nonzero wind acceleration. Simple time- and height-dependent parameterizations are developed for the eddy diffusivity and the slope-induced thermal wind v_T. The surface values of v_T are allowed to vary as a sine function of time, which is positive during the day and negative at night.

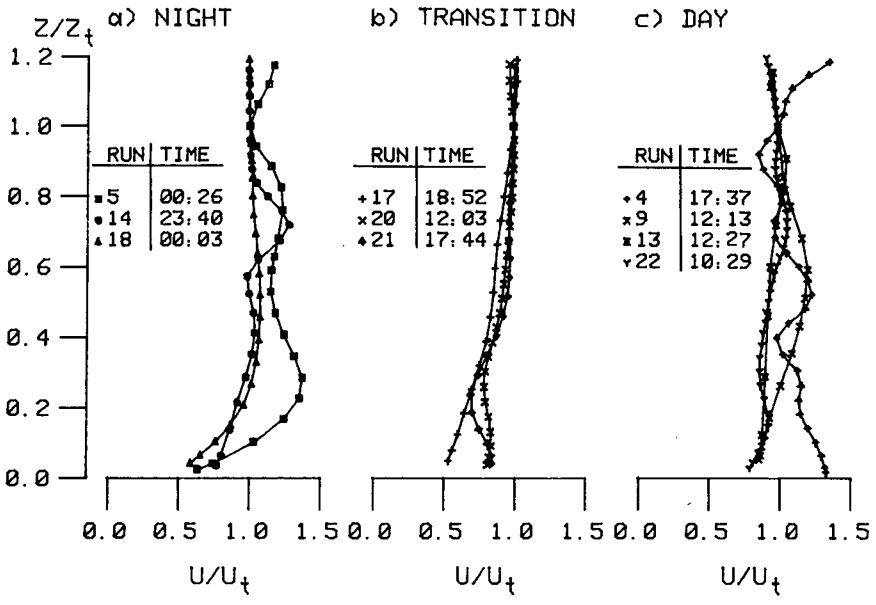

FIG. 10. Vertical profiles of wind velocity, classified into three stability classes. U_t-wind velocity at the top of the ABL.

The wind hodographs obtained from the 24-hour simulation of the model are shown in Fig. 11. Based on the model results, we are able to derive the following conclusions:

1) The simulated wind vector does not change its direction during the day and is parallel to the geostrophic wind on the top of the ABL. This can explain the uniform shape of the daytime hodographs in Fig. 8.

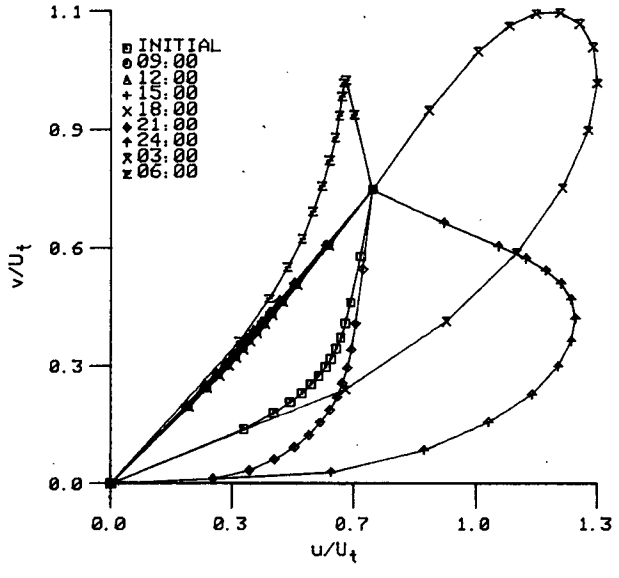

FIG. 11. Wind hodograph obtained by 24-hour simulation of the model. U_t-wind velocity at the top of the ABL.

2) The simulated nighttime hodographs in Fig. 11 have a spiral shape. This also agrees with the shape of the hodographs plotted in Fig. 8. The strongest "low-level jet" is obtained about 21 hours after the beginning of the simulation, equivalent to 0300 LST. This cannot be compared with our data, since the observations at this time were not performed during our experiment. This could explain, though, why the wind maxima at night, presented in Fig. 10a, are not very pronounced. The simulated surface wind at night is further downslope as a simultaneous effect of the gravity (thermal wind v_T) and stability factors (increase of the cross-isobar angle). This again is in agreement with Fig. 8.

3) The results of the simulation depicted in Fig. 11 were obtained with the assumption that the synoptic thermal wind is zero. We also performed a numerical experiment (not shown) with the nonzero synoptic thermal wind of the magnitude 5 m s^{-1}/km in a 200 m-deep layer (which is equivalent to the horizontal temperature gradient about 1.5 K/100 km). We found that synoptic baroclinicity modifies the wind hodographs very slightly in the shallow ABL. From this we conclude that the irregularities of the daytime hodographs on the top of the ABL, seen in Fig. 8, should be explained as an effect of the secondary circulation, rather than synoptic baroclinicity. The model results presented by Brown (1981) are quite similar to our daytime hodographs in Fig. 8. Brown argues that the presence of the secondary circulations is ensured if the surface velocity exceeds 5 m s^{-1} and the stratification is weakly unstable.

4) The results of the steady-state version of the model, shown in Fig. 12, indicate that the explanation of the wind directional constancy with height by the

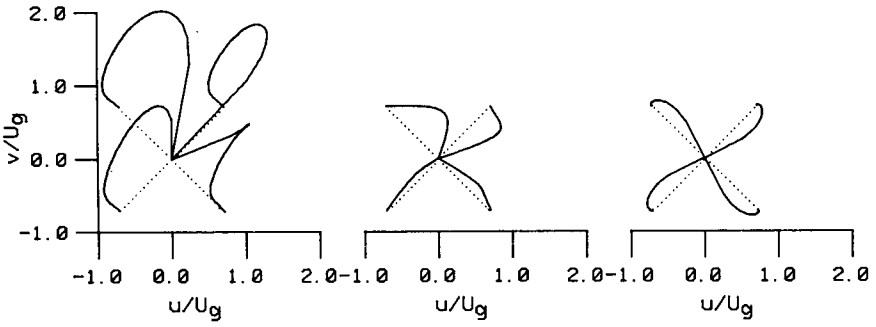

FIG. 12. Hodographs of the wind vectors obtained from the steady-state version of the model for different orientations of the geostrophic wind vectors. A test of the role of the main factors influencing the flow over Antarctica: (i) $v_T = -15$ m s^{-1}; $k_0 = 1$ m^2 s^{-1}, (ii) $v_T = -15$ m s^{-1}; $k_0 = 20$ m^2 s^{-1}, and (iii) $v_T = +1$ m s^{-1}; $k_0 = 1$ m^2 s^{-1}. Dots indicate the direction of the geostrophic winds at the top of the ABL. x-axis of the coordinate system is oriented downslope. Eddy diffusivity, $k = k_n$.

mechanism described by Mahrt and Schwerdtfeger (1970) is satisfactory during the winter time. This explanation fails, however, during the summer when more intensive turbulent mixing and positive thermal wind can occur during the day. Therefore, only the height persistency in the direction of the geostrophic flow (synoptic forcing) can explain the constancy of the surface winds during the polar summer.

6. Conclusions

In this paper vertical profiles of the temperature and the wind vector over Antarctica were presented and discussed. The temperature profiles, characteristic for the polar summer, have shown a well-developed mixed layer during the day and a strong inversion layer at night. It was deduced that due to the duration of the day and night, the daytime ABL is quasi steady state, with an entrainment rate of $w_e \sim 5.6 \times 10^{-3}$ m s^{-1}, and the nocturnal ABL is shallow and nonsteady.

During the day, when the surface inversion had vanished the flow was downslope, due to the weak intensity of the surface radiational heating and synoptically driven circulation toward the edge of the continent.

During the night, regular spiral-like wind hodographs were observed. In contrast, the daytime hodographs did not have a spiral shape and were found to be very irregular on the top of the ABL.

Acknowledgments. The study was supported by the National Science Foundation Grant (DPP 81-00161). Our thanks go to the participants of the U.S. Antarctic Research Program, as well as Expeditions Polaires Francaises (Dr. J. Vaugelade and Mr. R. Guillard). Our appreciation is also addressed to Drs. G. Weller and J. Gosink for their valuable comments. Our special thanks are dedicated to all the other members of the traverse team whose helpfulness and dedication made this work not only possible, but very delightful. They are: C. Busicchia, P. Laffont, B. Piccot, M. Pourchet, M. Savage, D. Simon and J. Wiget.

APPENDIX

A Simple Numerical Model of Flows over Antarctica

This simple model is based on the following set of equations, which describes the distribution of the wind velocity in the nonsteady ABL over a slightly inclined terrain (the nonsteady version of the equations derived by Sorbjan, 1983, and written for the Southern Hemisphere).

$$\left.\begin{aligned} \frac{\partial u}{\partial t} + f(v - v_{g0}) - fz\frac{\partial v_g}{\partial z} + fv_T &= \frac{\partial}{\partial z}k\frac{\partial u}{\partial z} \\ -\frac{\partial v}{\partial t} + f(u - u_{g0}) - fz\frac{\partial u_g}{\partial z} &= -\frac{\partial}{\partial z}k\frac{\partial v}{\partial z} \end{aligned}\right\}, \quad \text{(A1)}$$

where

u, v, u_g, v_g components of the wind and the geostrophic wind vectors at an arbitary height and the surface;
u_{g0}, v_{g0}
f Coriolis parameter,
k eddy diffusivity,
$v_T = \beta\theta'\psi/f$ slope-generated thermal wind.

In Eq. (A1), it is assumed that the geostrophic wind can vary with height (synoptic baroclinicity).

Our model is designed to describe qualitatively the time variation of the wind in the ABL. This is achieved by adopting a very simple and somewhat arbitrary closure of Eq. (A1), for the eddy diffusivity k. Generally, the eddy diffusivity can be parameterized as follows:

$$k = \begin{cases} \kappa u_* z(1 - z/h)/(1 + 4.7\eta z/h) & \text{stable (Sorbjan, 1984)} \\ \kappa u_* z(1 - z/h) & \text{neutral} \\ 4k_{\max} z/z_i(1 - z/z_i) & \text{convective (Wyngaard, 1981),} \end{cases} \quad \text{(A2)}$$

where

h, z_i	heights of the stable and convective ABL,
k_{max}	maximum value of k in the convective ABL,
κ	von Kármán constant,
u_*	friction velocity,
$\eta = h/L$	stability parameter, (L—Monin-Obukhov length).

We generalize Eq. (A2) assuming:

$$k(Z, t) = \begin{cases} k_n/(1 + 4.7\eta Z) & \text{for nighttime ABL} \\ k_n k_m & \text{for daytime ABL,} \end{cases} \quad \text{(A3)}$$

where $k_n = k_0 Z(1 - Z)$ (neutral case, $k_0 = \kappa u_* H$), $k_m = 4k_{max}/k_0$, and $Z = z/H$; H is the height of ABL. We assumed in Eqs. (A3) that $H = 200$ m, $k_0 = 20$ m^2 s^{-1}.

The time forcing in the model is expressed by the function F, which describes a diurnal variation of the eddy diffusivity and the thermal wind. We assumed $k_m(t) = [1 + cF(t)]$ with $c = 20$, and $\eta(t) = -15F(t)$. The function $F(t)$ is defined as:

$$F(t) = \begin{cases} \sin(2\pi t/T_1) & \text{for } 0 < t < T_1/2, \text{ daytime} \\ \sin\left[\pi\left(1 + \dfrac{t - T_1/2}{T_0 - T_1/2}\right)\right] & \text{for} \\ & T_1/2 < t < T_0, \text{ nighttime} \end{cases} \quad \text{(A4)}$$

where $T_0 = 24$ hours, $T_1/2 = 14$ hours.

The form of $F(t)$ indicates that we assume the day and night to be 14 hours and 10 hours long, respectively. This is in agreement with the net radiation distribution shown in Fig. 8.

In Eq. (A1), we also assume that

$$v_T = v_T(0)(e^{-Z} - e^{-1})/(1 - e^{-1}) \quad \text{(A5)}$$

where $v_T(0) = RF(t)$ and R is equal to 4.0 at night and 0.4 during the day. Notice that the thermal wind decreases exponentially from the value $v_T(0)$ at the surface to zero at the top of the ABL. This can be compared with the profile of v_T shown in Fig. 10. The exponential shape of v_T was also assumed by Mahrt and Schwerdfeger (1970). The other parameters in Eq. (A1) are chosen to be $u_{g0} = 5$ m s^{-1}, $v_{g0} = 5$ m s^{-1}, $f = -1.2 \times 10^{-4}$ s^{-1}.

The boundary conditions are established as:

$$\left.\begin{aligned} u &= 0 \\ v &= 0 \end{aligned}\right\} \quad \text{for} \quad z = 0$$

$$\left.\begin{aligned} u &= u_{g0} + \frac{\partial u_g}{\partial z} H \\ v &= v_{g0} + \frac{\partial v_g}{\partial z} H \end{aligned}\right\} \quad \text{for} \quad z = H. \quad \text{(A6)}$$

As an initial condition, we use the steady state solution of Eq. (A1), with $k = k_n$ and $v_T(0) = 0$. To solve Eq. (A1), we first transform it to the form:

$$\frac{\partial W}{\partial t} = \frac{\partial}{\partial Z} k \frac{\partial}{\partial Z} W - f(v_T + i\Lambda Z)e^{ift}, \quad \text{(A7)}$$

where

$$W = [(u - iv) - (u_{g0} - iv_{g0})]e^{ift}$$

$$\Lambda = \left[\frac{\partial u_g}{\partial Z} - i\frac{\partial v_g}{\partial Z}\right],$$

and then express Eq. (A7) in the finite difference form. The finite differences algebraic equations were solved by the "tridiagonal algorithm," described in Appendix A of Roache (1972).

REFERENCES

Andre, J. C., and L. J. Mahrt, 1982: The nocturnal surface inversion and influence of clear-air radiative cooling. *J. Atmos. Sci.*, **39**, 864–878.

Artemyev, A. N., 1972: Structure of the atmospheric boundary layer in central Antarctica. *Sov. Antarct. Exped. Inf. Bull.*, **84**, 311–316.

Arya, S. P. S., 1981: Parameterizing the height of the stable atmospheric boundary layer. *J. Appl. Meteor.*, **20**, 1192–1202.

——, 1982: Atmospheric boundary layer over homogeneous terrain, *Engineering Meteorology*, E. J. Plate, Ed., Elsevier, 233–267.

Ball, F. K., 1957: The katabatic winds of Adelie Land and King George V. Land. *Tellus*, **9**, 201–208.

Brown, R. A., 1981: On the use of exchange coefficients in modelling turbulent flow. *Bound.-Layer Meteor.*, **20**, 111–116.

Caughey, S. J., J. C. Wyngaard and J. C. Kaimal, 1979: Turbulence in the envolving stable boundary layer. *J. Atmos. Sci.*, **36**, 1041–1052.

Cerni, T. A., and T. R. Parish, 1984: A radiative model of the stable nocturnal boundary layer with application to the polar night. *J. Climate Appl. Meteor.*, **23**, 1563–1572.

Dalrymple, P. C., and L. A. Stroschein, 1966: Antarctic plateau radiation climatology. *Antarct. J. U.S.*, **1**, 199.

Deardorff, J. C., and G. E. Willis, 1974: Computer and laboratory modeling of the vertical diffusion of nonbouyant particles in the mixed layer, *Advances in Geophysics*, Vol. 18B, Academic Press, 187–200.

Delaunay, D., and A. Poggi, 1981: Variations du vent et de la temperature de l'air en zone cotiere de Terre Adelie. *La Meteorologie*, **6**(24), 61–79.

Gosink, J., 1982: Measurements of katabatic winds between Dome C and Dumont d'Urville. *Pure Appl. Geophys.*, **120**, 503–526.

Kuhn M., and H. H. Lettau and A. J. Riordan, 1977: Stability-related wind spirals in the lowest 32 meters. Meteor. studies at Plateau Station, Antarctica. Pap. 7, *Antarct. Res. Ser.*, **25**, 93–111.

Lettau, H. H., and W. Schwerdtfeger, 1967: Dynamics of the surface wind regime over the interior of Antarctica. *Antarct. J. U.S.*, **2**(5), 155–158.

——, A. J. Riordan and M. Kuhn, 1977: Air temperature and two-dimensional wind profiles in the lowest 32 meters as a function of bulk stability. Meteor. Studies at Plateau Station, Antarctica, Paper 6, Antarctic Res. Series, 25, Amer. Geophys. Union, 77–91.

Mahrt, L. G., and W. Schwerdtfeger, 1970: Ekman spirals for exponential thermal wind. *Bound.-Layer Meteor.*, **1**, 137–145.

Mather, K. B., and G. S. Miller, 1967a: The problem of katabatic wind on the coast of Terre Adelie. *Polar Rec.*, **4**(8), 425–432.

——, and ——, 1967b: Notes on topographic factors affecting the surface wind in Antarctica with special reference to katabatic winds and bibliography. University of Alaska Tech. Rep. UAG-R-189:125.

Poggi, A., J. Andre, G. Wendler, P. Blaix, D. Delaunay, J. Gosink and Y. Kodama, 1982: Interaction atmosphere-glace–ocean en Antarctique. *La Meteorologie,* **6,** 163–171.

Radok, U., 1973: On the energetics of surface winds over the Antarctic ice cap. Energy fluxes over polar surfaces. *Proc. IAMAP, IAPSO/ SCAR/WMO Symp.,* Moscow, WMO Tech. Note 179, 2–5.

Riordan, A. J., 1977: Variations of atmosphere and air motion in 0 to 32 meter layer at Plateau Station, Antarctica. Meteor. Studies at Plateau Station, Antarctica, Pap. 8, *Antarct. Res. Ser.,* **25,** 113–127.

Roache, P. J., 1972. Computational fluid dynamics, Hermosa Publishers, 434 pp.

Schwerdtfeger, W., 1970: The climate of the Antarctic. *World Survey of Climatology* H. E. Landsberg, Ed., Elsevier, 235–355.

Sennequier, G., D. Cheymol and D. Martin, 1984: Note de travel de l'Establissement d'etudes et de Recherches Meteorlogiques, 3. Programme I.A.G.O. Catabatique. Secretariat d'Etat Aupres du Ministre de l'Urbanisme du Logement et des Transports, Charge des Transports, Direction de la Meteorologie, 111 pp.

Sorbjan, Z., 1983: Rossby number similarity in the atmospheric boundary layer over slightly inclined terrain. *J. Atmos. Sci.,* **40,** 718–728.

——, 1984: A model study of the stably stratified steady–state atmospheric boundary layer over a slightly inclined terrain. *J. Atmos. Sci.,* **41,** 1863–1874.

Wendler, G., and Y. Kodama, 1984: On the climate of Dome C, Antarctica, in relation to its geographical setting. *J. Climatol.,* **4,** 495–508.

——, —— and A. Poggi, 1983: Katabatic wind in Adelie Land. *Antarct. J. U.S.,* **18**(5), 201–203.

Wentzel, P. J., 1982: Toward parameterization of the stable boundary layer. *J. Appl. Meteor.,* **21,** 1–13.

Wyngaard, J. C., 1981: Wind shear in the baroclinic convective PBL. *Proc. Symp. on Turbulence, Diffusion and Air Pollution,* Atlanta, 78–79.

Yamada, T., 1979: Prediction of the nocturnal surface inversion height. *J. Appl. Meteor.,* **18,** 526–531.